Available online at www.sciencedirect.com
SCIENCE DIRECT®
Journal of the European Ceramic Society 25 (2005) 1025–1031
www.elsevier.com/locate/jeurceramsoc

The resistance to oxidation of an HfB_2–SiC composite

Frédéric Monteverde*, Alida Bellosi

Institute of Science and Technology for Ceramics, National Research Council, Via Granarolo 64, 48018 Faenza, Italy

Received 12 March 2004; received in revised form 12 May 2004; accepted 15 May 2004
Available online 22 July 2004

Abstract

The oxidation resistance of an hot-pressed HfB_2–SiC composite was studied through non-isothermal and isothermal treatments at temperatures up to 1600 °C in air. The most severe oxidation conditions consisted of repeated heating-cooling cycles at 1600 °C for up to 80 min of exposure. A thermogravimetric test for over 20 h at 1450 °C provided evidence that, at this temperature, the oxidation kinetics fits a paralinear law until 10 h, when a partial rupture of external oxide scale occurs (i.e. a break-away reaction). Afterwards, the weight gain data fit a linear law. The main secondary phases formed in the composite during hot-pressing, namely BN, Hf(C,N) and a Si-based compound, although in limited amounts, influenced the oxidation resistance at temperatures below 1350 °C. At temperatures higher than about 1400 °C, the presence of SiC particles markedly improved the oxidation resistance due to the formation of a protective borosilicate glassy coating on the exposed surfaces.

Keywords: Hot-pressing; Composites; HfB_2; Microstructure; Oxidation resistance; SiC

1. Introduction

Ultra-high temperature ceramics (UHTCs), particularly diborides and carbides of the transition metals like hafnium and zirconium, are currently accepted as potential candidates for a variety of high-temperature structural applications, including furnace elements, plasma-arc electrodes, or rocket engines and thermal protection structures for space vehicles with temperature capabilities at over 1800 °C.[1–3] The growing interest in UHTCs stems from the opportunities they provide for designing a new generation of space vehicles with very sharp leading edges.[4] This innovative class of materials has the potential to overturn an age-old tenet of aerodynamics, that only blunt-body spacecraft can survive the searing temperatures generated as the vehicle repeatedly tears through the terrestrial atmosphere during hypersonic flights. The expected highly localized heating loads in the areas particularly exposed to the interaction with the atmosphere during re-entry missions dictate the need for oxidation and ablation resistance, coupled with a low surface catalytic efficiency, and a capacity to conduct away or re-radiate excess energy.[5] The introduction of SiC in matrices of zirconium and hafnium diborides improved the mechanical properties[1,3,6] and oxidation resistance.[3,7–9]

Existing research activities are still facing technological difficulties in scaling-up the manufacturing of near net-shape dense components. Sintering conditions of elevated temperatures and pressure[3,4] induce coarsening of the microstructure and a general degradation in the mechanical properties. The addition of sintering aids have proven to be a suitable route to improving the sinterability and to controlling development of the microstructure during the densification of refractory diborides matrices.[6,9,10]

The present study deals with an HfB_2–SiC composite (containing 5.8 v/o Si_3N_4 as sintering aid) hot-pressed at 1850 °C for 20 min. The oxidation behavior in ambient air was studied by monitoring the weight change, according to different thermal treatments. Modifications in the microstructure were examined and correlated to the oxidation mechanisms involved.

2. Experimental

2.1. The fabrication of the material

The starting powder mixture, of composition (v/o) HfB_2 + 19 SiC + 5.8 Si_3N_4, was milled for one day in a

* Corresponding author. Fax: +39 0546 463 81.
E-mail address: fmonte@istec.cnr.it (F. Monteverde).

0955-2219/$ – see front matter © 2004 Elsevier Ltd. All rights reserved.
doi:10.1016/j.jeurceramsoc.2004.05.009

Table 1
Thermomechanical properties of the composite: Vickers microhardness Hv1.0, fracture toughness (chevron notch method) K_{IC}, linear thermal expansion coefficient λ, 4-pt flexural strength (at different temperatures) σ

Hv1.0 (GPa)[a]	K_{IC} (MPa$\sqrt{m}$)[a]	λ (10^{-6} °C^{-1})			σ (MPa)[a]			
		25–1000 °C	25–1200 °C	25–1300 °C	25 °C	1200 °C	1400 °C	1500 °C
20.4 ± 0.6	4.3 ± 0.1	7.24	7.37	7.30	560 ± 100	380 ± 50	280 ± 20	150 ± 5

[a] Mean ± 1 S.D.

polyethylene jar using absolute ethanol and silicon nitride balls, and then dried and sieved. The as-processed powder batch was hot-pressed at 1850 °C for 20 min and 30 MPa of applied pressure, using an induction-heated BN-lined graphite die. Some properties of the composite are listed in Table 1. Details concerning the densification behavior, microstructure and thermomechanical properties of the composite are reported elsewhere.[10]

2.2. The oxidation treatments

The composite was subjected to various oxidation treatments (at ambient pressure), namely:

(A) Non-isothermal run up to 1450 °C in flowing dry air (50 cm^3/min), heating rate 2 °C/min and free cooling.
(B) Isothermal runs at 1170 °C, 1250 °C, 1350 °C and 1500 °C for 1 h (loading and removal of the sample at the fixed set-point). After the loading of the test piece, the furnace took up to 10 min to reach the desired temperature.
(C) Isothermal run at 1450 °C for 20 h in flowing dry air (50 cm^3/min), heating rate 30 °C/min and free cooling.
(D) Isothermal runs at 1600 °C for 20, 40 and 80 min of exposure (loading and removal of the coupon at the fixed set-point for each scheduled exposure). After the loading of the test piece, the furnace took 15 min to reach the temperature of 1600 °C.

Coupons with dimensions of 2.5 mm × 2.0 mm × 10.0 mm (for treatments A–C–D) and dimensions of 10 mm × 10 mm × 1 mm (for treatment B) were cut out from the sintered billet (surface finish $R_a \sim 0.2$ μm), washed in an ultrasonic bath of acetone, and dried at 80 °C overnight. Treatments A and C were executed using a thermogravimetric analyzer (mod. STA409, NETZSCH Gerätebau GmbH, Germany) equipped with a vertically heated Al_2O_3 chamber. The samples were placed on zirconia supports, separating them from the Al_2O_3 holder. The mass variation was recorded (10^{-3} mg of accuracy) over the scheduled thermal cycle. Treatments B and D were performed using a bottom-loading furnace box. The test piece was placed upon SiC supports with minimal contact area. The sample mass was measured before and after each cycle.

2.3. The analysis of the microstructure

The microstructure was analyzed with a scanning electron microscope (SEM, mod. S360, Cambridge, UK) equipped with an energy dispersive microanalyzer (EDX, mod. INCA Energy 300, Oxford Instruments, UK), and an X-ray diffractometer (XRD, mod. D500, Siemens, Germany). Sections of some oxidized coupons were first polished using diamond abrasives (finished 0.5 μm), and then observed via SEM-EDX analyses. The cross-sections were imaged using secondary electrons (SEs), free of conductive coating in order to maintain the sensitivity of the EDX equipment to the low *Z* elements as high as possible. The thickness of the oxidized specimens was measured (accuracy ± 2 μm) using an optical microscope.

3. Results

3.1. The microstructure of the hot-pressed composite

The bulk density of the hot-pressed material was 8.8 g/cm^3. The SEM observations of the fracture surface showed regularly shaped HfB_2 grains, 5 μm maximum in size, and SiC particles (Fig. 1). In addition, other (crystalline) phases were detected by XRD analysis: monoclinic HfO_2 and a cubic Hf(C,N) solid solution. The SEM-EDX examination of the polished section identified all the mentioned phases, but also highlighted some more minority compounds formed during hot-pressing, basically an Si-based phase and boron nitride, which are all located intergranularly (Fig. 2). EDX spectra from the main secondary phases are shown in Fig. 3. The SiC particulate, which represents the majority of the dark features in Fig. 2, is partly

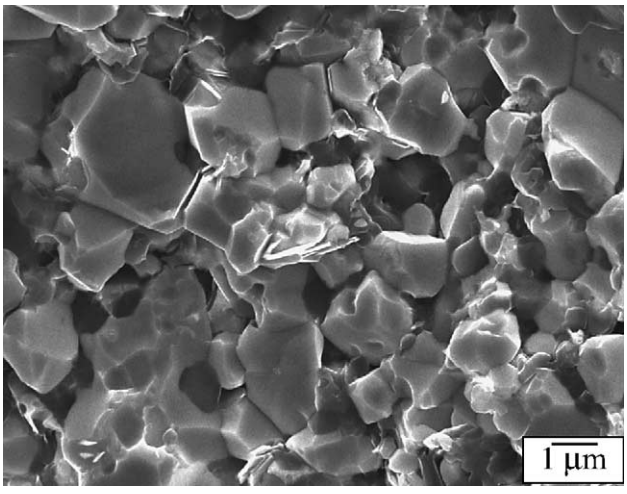

Fig. 1. SEs-SEM micrograph of a fracture surface.

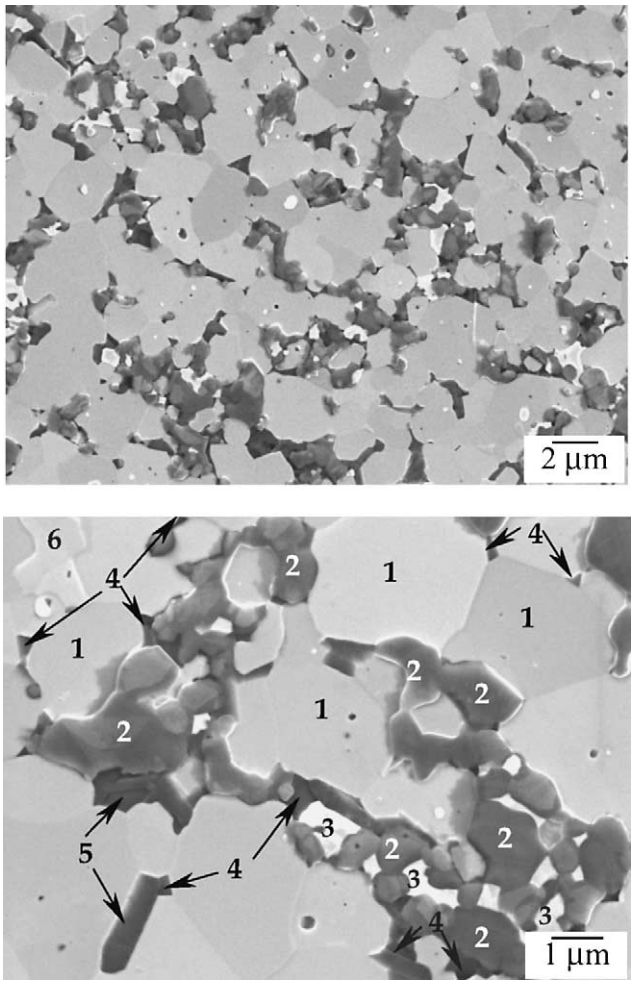

Fig. 2. SEs-SEM micrographs from polished sections. The phases HfB_2 (1), SiC (2), HfO_2 (3), Si-based compound (4), BN (5) and Hf(C,N) s.s. (6) are indicated.

distributed in a clustered formation. Residual porosity is not appreciable. The addition of a sintering aid like Si_3N_4 greatly favored densification of the HfB_2–SiC system, and near full density was achieved by applying an hot-pressing temperature of 1850 °C. The SiC particles hindered excessive growth of the diboride matrix and kept the average grain size at less than 2 μm. Details of the densification behavior and microstructure development are reported elsewhere.[10]

3.2. The oxidation behavior

The mass change versus temperature during treatment A is depicted in Fig. 4. Peculiar temperature values (T_1, T_{flex}, T_{min}, T_{max}) are indicated along the thermogravimetric (TG) curve. The wavy pattern of TG data is closely connected to the thermal instability of the oxide scale growing on the external faces of the oxidizing sample. The decreasing branch of the TG data between T_{min} and T_{max} is a typical behavior of diboride matrices already described for similar ZrB_2–SiC systems.[8]

Table 3
Treatment D: mass change W and thickness change dT

	20 min	2 × 20 min	4 × 20 min
W (mg/cm^2)	1.20 ± 0.05	2.00 ± 0.08	2.20 ± 0.08
dT (μm)	18	23	30

In the light of these results, four distinct temperatures were selected for treatment B in order to evaluate the behavior under isothermal conditions when different oxidizing regimes are active. In spite of the low mass gain measured in all the cases, an apparent oxidation constant K_P was calculated, under the hypothesis of a parabolic law (Table 2). The thickness change of the oxidized samples are reported as well.

The cumulative mass gains after treatment D (Table 3) provided evidence of deceleratory kinetics.

The mass gain during the isothermal test at 1450 °C for 20 h (treatment C) is shown in Fig. 5. An offset equal to 0.15 mg/cm^2, which accounts for the oxidation preceding the planned exposure, was subtracted from the TG data. A deviation from the monotonically decreasing trend of the TG curve was registered just before 10 h of exposure. This event was regarded as a special kind of break-away reaction. After 10 h of exposure, a linear equation describes further oxidation of the material. The TG data for up to 10 h of exposure, elaborated on the basis of the multiple-law model proposed by Nickel,[11] indicate that the process follows a paralinear law. The most relevant outputs are that the oxidation process is rate-limited by diffusional mechanisms and that the linear contribution is negative.

3.3. Microstructural changes after oxidation treatments

The collection of micrographs in Fig. 6 shows some microstructural modifications of the sample surface after treatment B. At 1170 °C, glassy silica-based islands and widespread tiny hafnia crystals cover the external faces of the oxidized sample. At 1250 °C, the coverage of the glassy coating becomes more regular. What is more, the bursting of bubbles serves to record the evolution of gaseous oxidation products: in fact, in correspondence to T_{min} (Fig. 4),

Table 2
Treatment B: mass change W (K_P apparent parabolic constant, $W^2 = K_P t$, t is time of exposure), and thickness change dT.

	1170 °C	1250 °C	1350 °C	1500 °C
W (mg/cm^2)	0.45 ± 0.03	0.50 ± 0.03	0.65 ± 0.03	1.60 ± 0.05
K_P (mg^2/cm^4/h^1)	0.2	0.25	0.42	2.56
dT (μm)	None	None	−8	20

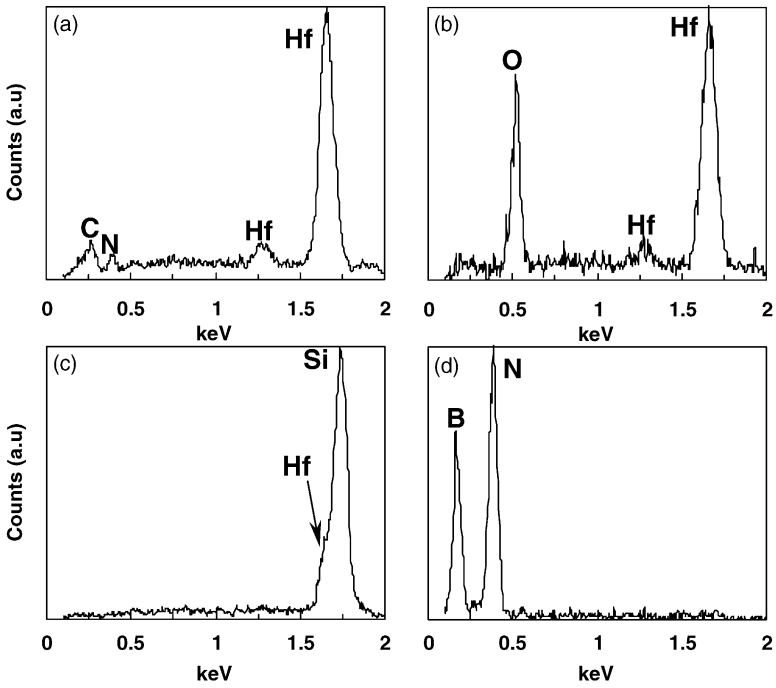

Fig. 3. EDX spectra (5 keV of electron beam energy) from Hf(C,N) s.s. (a), HfO_2 (b), Si-based compound (c), and BN (d).

the loss of gases dominates the mass change behavior. At 1350 °C, a glassy layer is still present on the surface and partially protects the sample from oxidation. A decrease in the thickness of the oxidized sample was measured (Table 2). Raising the temperature up to 1500 °C, a single bubble occupies one of the largest external faces of the piece. The unoccupied regions were basically protected by hafnium oxide crystals floating inside a thick glassy scale, whilst a porous layer consisting of hafnium oxide grew under the bubble. At this temperature, the thickness of the oxidized specimen increased (Table 2). The XRD analysis of the oxidized surface, after the removal of the bubble, confirmed the presence of monoclinic hafnia.

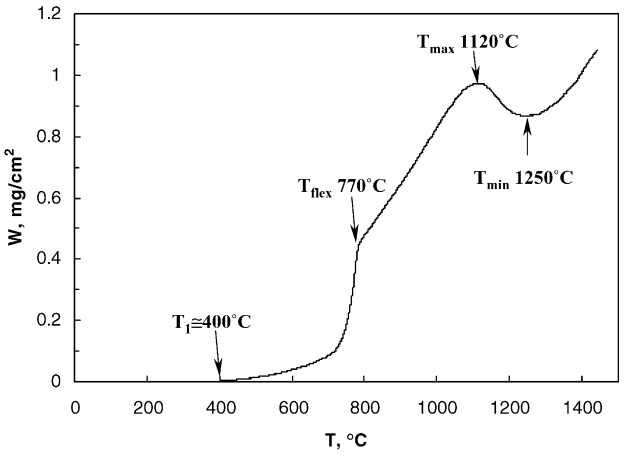

Fig. 4. Weight change (W) vs. temperature (T) during the non-isothermal run up to 1450 °C in flowing dry air. Temperatures T_1, T_{flex}, T_{max} and T_{min} are indicated.

As far as treatment D is concerned, the micrographs in Fig. 7 illustrate how little the microstructure changed after the short repeated exposures at 1600 °C. The depth of corrosion in fact did not exceed 25 μm after the longer exposure. The measurements of the final thickness of the as-oxidized samples show values greater than the initial one (Table 3).

After treatment C, the XRD analysis of the oxidized surface detected highly textured monoclinic HfO_2 and $HfSiO_4$. Moreover, the characteristic hump in the XRD pattern denotes the existence of a glassy product. The examination via SEM-EDX of a polished cross-section showed a layered configuration (Fig. 8). The basic scheme consists of a thin

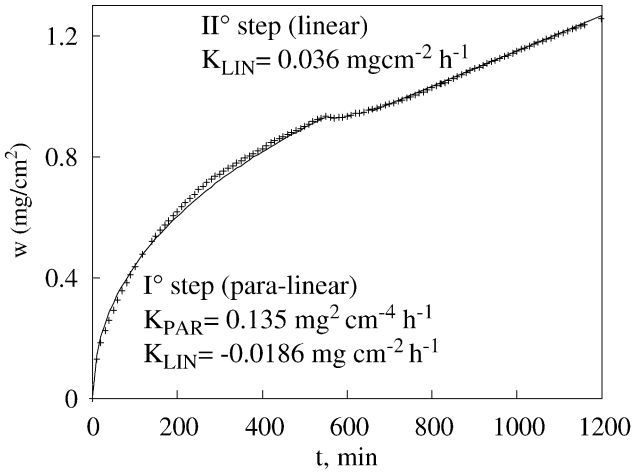

Fig. 5. Weight change (W) vs. exposure time (t) for 20 h at 1450 °C. In accordance to a paralinear model, $W = K_{PAR}\sqrt{t} + K_{LIN}t$, single parameters and fitting curve (up to about 10 h) are shown. A linear pattern fits the remanent TG data (II° step).

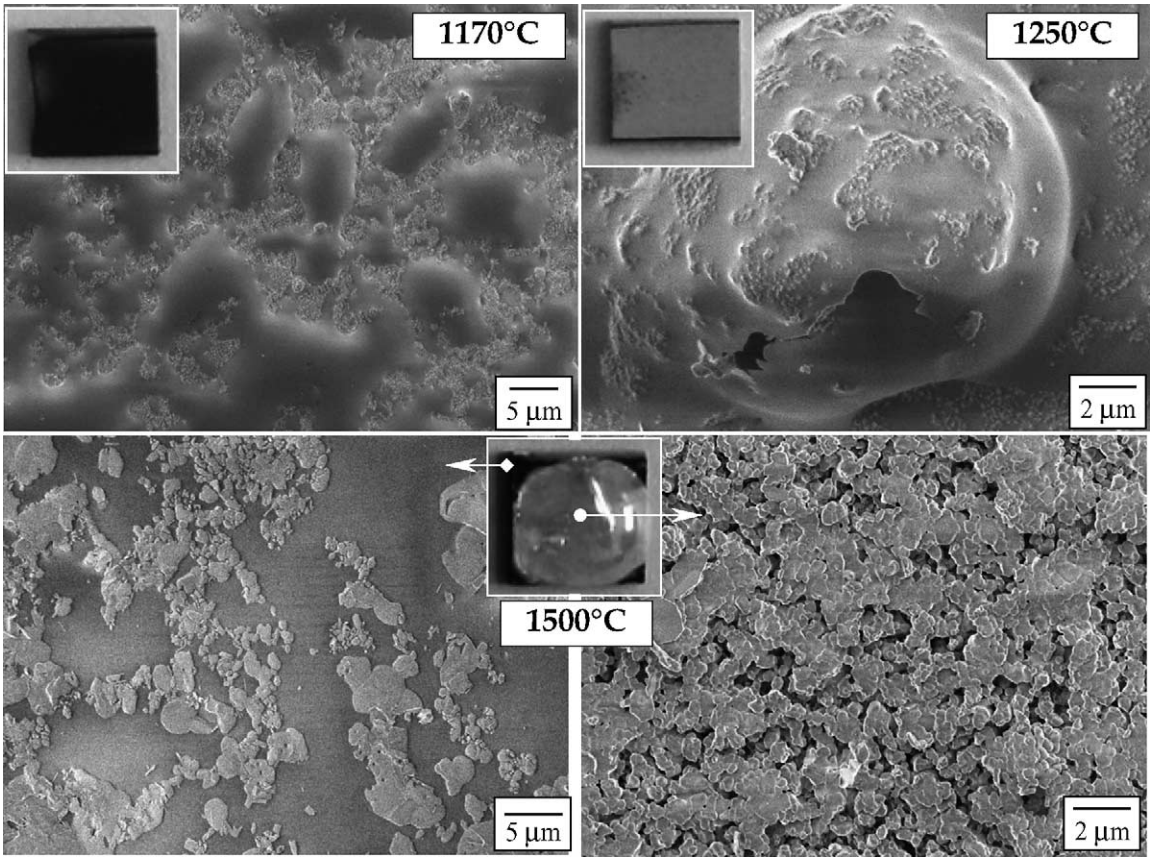

Fig. 6. SEs-SEM micrographs from the oxidized surfaces, after treatment B. The inset photos show the visual look of the treated samples.

outermost glassy layer covering a relatively porous oxide scale, 10 μm thick, that contains HfO_2 and $HfSiO_4$ polycrystals embedded in a glassy melt. Underneath, a 100 μm thick intermediate layer is characterized by traces of corrosion extending up to the interface between the corroded/virgin material. Little localized spallation of the external oxide scale was observed. The EDX analysis of the glass basically identified the chemical composition of the silica. Neither elemental hafnium nor carbon were detected. The presence of boron in the glass remained unclear, most likely below the detection limit of the analytical technique used. Several SiC particles lying close to the external oxide layer appear only slightly affected by the oxidation attack. The central part of the intermediate layer reveals more apparent traces of the oxidation attack in the form of an incipient porosity (Fig. 8).

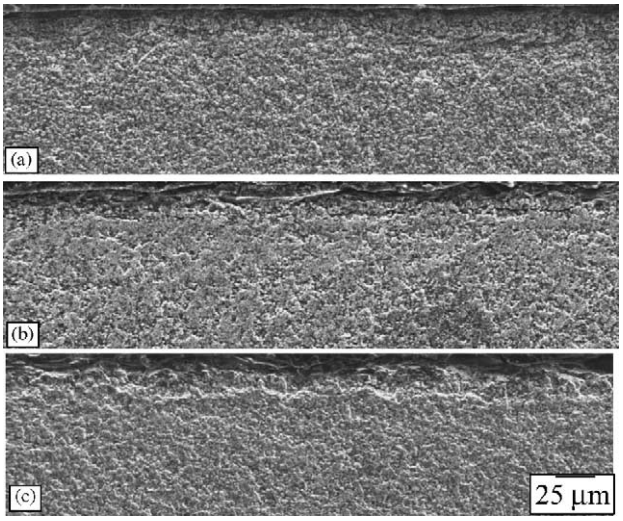

Fig. 7. SEs-SEM micrographs of cross sections, cut out from coupons after treatment D: 20 min (a), 2 × 20 min (b), and 4 × 20 min (c). The upper dark zone in each micrograph is occupied by resin.

4. Discussion

Depending on the selected temperature range, the expected main reactions describing the oxidation process involve either mass gain (reactions 1–4) or mass loss (reactions 5–7):

$$HfB_2 + \tfrac{5}{2}O_2 = HfO_2 + B_2O_3\,(l) \quad (1)$$

$$SiC + \tfrac{3}{2}O_2 = SiO_2 + CO\,(g) \quad (2)$$

$$2BN + \tfrac{3}{2}O_2 = B_2O_3\,(l) + N_2\,(g) \quad (3)$$

$$HfC_{1-x}N_x + \tfrac{3-x}{2}O_2 = HfO_2 + (1-x)CO\,(g) + \tfrac{x}{2}N_2\,(g) \quad (4)$$

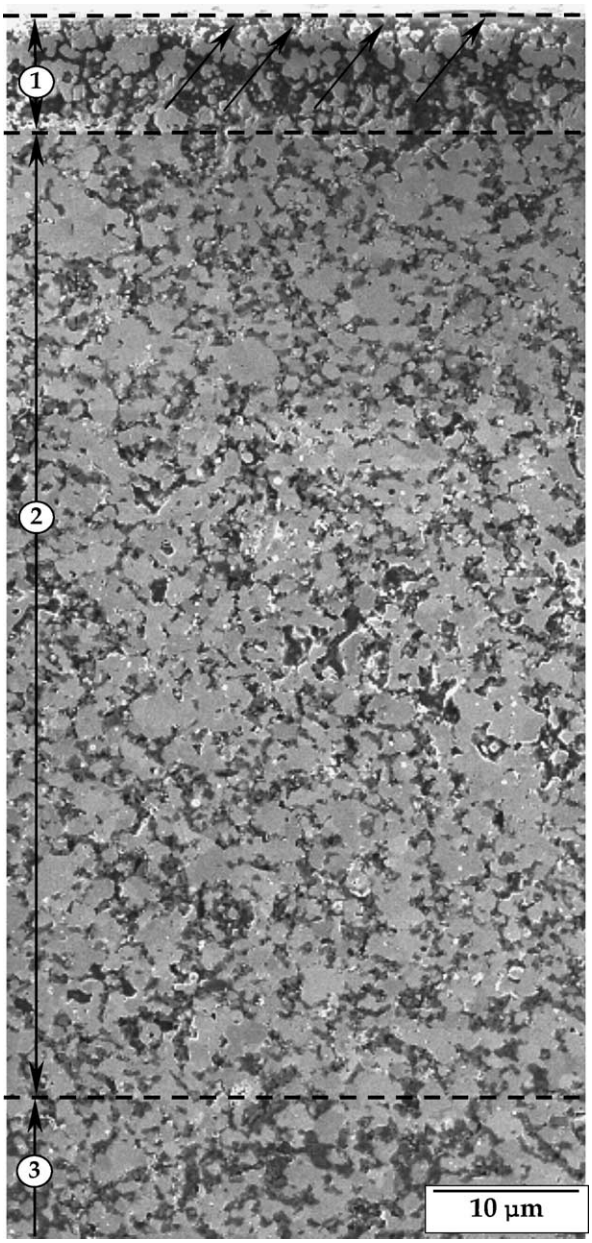

Fig. 8. Collage of SEs-SEM micrographs from a cross section of the composite, after being oxidized accordingly to treatment C: 1→, external oxide scale; 2→, intermediate scale; 3→, unreacted bulk. Oblique black arrows indicate the outermost thin glassy film.

$$B_2O_3\,(l) = B_2O_3\,(g) \quad (5)$$

$$SiO_2\,(s) + CO\,(g) = SiO\,(g) + CO_2\,(g) \quad (6)$$

$$2SiO_2\,(s) + SiC\,(g) = 2SiO\,(g) + CO\,(g). \quad (7)$$

All, or some of them, may be simultaneously active. Other equilibrium equations, candidate mechanisms for the formation/decomposition of silica, were omitted for the sake of brevity.[13] The oxidation products of HfB_2 are HfO_2 and amorphous B_2O_3. The latter compound is known to have a melting point of 450 °C and an high vapor pressure, so at high temperatures it readily vaporizes. The abrupt increase in the scaling rate above 700 °C (Fig. 4) is primarily due to a selective oxidation of either HfB_2 (reaction 1) or the secondary phases (reactions 3 and 4), with no appreciable attack of the SiC particles. The hafnium carbonitride grains directly facing or near the ambient atmosphere, for instance, oxidize, forming a porous thin scale. Such a scale does not limit the diffusion of oxygen through interconnected pores or via lattice vacancies in the HfO_2 which is recognized as an anionic conductor. At the same time, the fluid B_2O_3 does not significantly hinder oxidation. Moreover, the grain boundary silicon-containing phase oxidizes, reacts with the available B_2O_3, promoting the formation of a borosilicate glass with higher melting point, lower vapor pressure and viscosity than B_2O_3 alone. Such a glass starts plugging pores and acts as a barrier against the inward diffusion of oxygen more efficiently than B_2O_3 and HfO_2. The mild slowdown of the TG curve above 800 °C in Fig. 4 may be ascribed to better protection against oxidation. The decreasing trend of the TG data between T_{min} and T_{max} (Fig. 4) primarily accounts for the loss of the B_2O_3 (g) component from the borosilicate glass.

Concrete advantages from the presence of SiC particles only result at temperatures above 1400 °C. In effect, the negative thickness change in the specimen oxidized at 1350 °C for 1 h after treatment B (Table 2) suggests that the outer glassy coating is unable to protect the material completely against oxidation, and a partial removal of the surface material occurs. Furthermore, at 1350 °C, the secondary Si-based phase represents the principal source of silicon for the borosilicate glass, but the small amount of this compound is inadequate to develop an external thick glassy scale.

On the contrary, increasing the temperature up to 1600 °C, the notable provision of silica due to an enhanced oxidation of SiC thickens the external glassy scale, which better limits the inward diffusion of oxygen. In addition, positive thickness changes at 1600 °C (Table 3) suggest that the presence of SiC actively contributed to prevent the dimensional recession that the studied system had at 1350 °C.

The multilayered corroded structures resulting from the isothermal treatment C (Fig. 8) basically agree with the evidence of Hinze et al.[13] who studied the oxidation of an (88% dense) HfB_2–SiC composite (in flowing pure oxygen) and indicated the diffusion of oxygen through the silica glass as the rate-limiting step accounting for the parabolic kinetics. In the present case, the oxidation behavior is adequately described with a paralinear equation (Fig. 5). The negative linear contribution accounts for volatile products, most likely fractions of B_2O_3 (reaction 5) or SiO_2 (reactions 5 and 6) being released from the outermost borosilicate layer. Additionally, the parabolic contribution explains the growth of an external oxide scale, which progressively imposes longer diffusion paths on oxygen arriving at the diboride–oxide interface. It is believed that a number of SiC particles are present at or near the ambient/hafnia interface following the transitory heating stage. At 1450 °C, in accordance with

reaction 2, a significant amount of silica combines with the available B_2O_3, forming a borosilicate glass that spreads laterally and across the hafnia grains surface, and composes a thick layer more protective than hafnia alone. Similar to other ZrB_2–SiC systems,[3,8,14] the high wetting angle between the borosilicate glass and HfO_2 ensures a regular coverage of the exposed faces. The behavior of the curve in Fig. 5 was regarded as a special kind of break-away reaction occurring after about 10 h of exposure. It supposedly derives from localized ruptures of the external oxide scale, chiefly in correspondence to burst bubbles, which locally lift off portions of the external oxide scale. The emergence of spalling events opens new accesses for oxygen into the bulk, and therefore impairs the protective role of the external oxide scale. Above 10 h of exposure, the linear pattern accounts for chemical reactions at the diboride–oxide interfaces as the rate-limiting step governing the resistance to oxidation.

Grain boundaries play the role of preferential paths for the inward transport of oxygen, and contemporaneously the outward migration of boron and silicon. The presence of SiC as intergranular particulate is certainly responsible for the good oxidation resistance. The evidence of residual unoxidized SiC particles within the partially oxidized interlayer (Fig. 8) settles the fundamental role of such a phase in suppressing the advance of the oxidation attack above 1400 °C. In a previous work, the oxidation resistance up to 1600 °C of an hot-pressed ZrB_2 ceramic (doped with 5 v/o Si_3N_4) improved by adding 20 v/o SiC in the same ZrB_2–Si_3N_4 formulation.[9]

In the light of the results from Levine et al. who studied the oxidation of an hot-pressed ZrB_2 + 20 v/o SiC material,[15] the formation of porosity in the middle of the intermediate scale (Fig. 8) can be attributed to a partial depletion of SiC. In fact, at high temperature and reduced oxygen partial pressure, the consumption of SiC by active oxidation [12] should be taken into due consideration.

5. Conclusions

An highly dense HfB_2–SiC composite, containing 5.8 v/o Si_3N_4 as sintering aid, was successfully fabricated by hot-pressing. The resistance to oxidation was tested by applying several heat treatments in laboratory air, monitoring not only the weight change but also the modifications to the microstructure induced by the oxidation. The thermogravimetric data for an isothermal test at 1450 °C agreed with a paralinear law over 10 h of exposure. Afterwards, linear kinetics seemed to prevail. The main oxidation products were HfO_2 and a borosilicate glass. The release of volatile oxidation products had an appreciable impact for the thermal treatments below 1350 °C. Above 1400 °C, the presence of the SiC particles markedly improved the oxidation resistance of the composite, because the oxidation of SiC provides significant amount of silica, forming a thick protective borosilicate glass. This glassy coating plugs pores, covers the sample surfaces and efficaciously seals grain boundaries depleted of the original secondary phases.

Acknowledgements

The authors acknowledge the very valuable support of the colleague Dr. A. Balbo for the thermogravimetric tests and D. Dalle Fabbriche for the hot-pressing.

References

1. Upadhya, K., Yang, J-M. and Hoffman, W. P., Materials for ultra-high temperatures structural applications. *Am. Ceram. Soc. Bull.* 1997, **58**, 51–56.
2. Wang, C. R., Yang, J.-M. and Hoffman, W. P., Thermal stability of refractory carbide/boride composites. *Mater. Chem. Phys.* 2002, **74**, 272–281.
3. Opeka, M., Talmy, I. G., Wuchina, E. J., Zaykoski, J. A. and Causey, S. J., Mechanical, thermal and oxidation properties of refractory hafnium and zirconium compounds. *J. Eur. Ceram. Soc.* 1999, **19**, 2405–2414.
4. Bull, J., White, M. J. and Kaufman, L., *Ablation Resistant Zirconium and Hafnium Ceramics*. US Patent 5,750,450 (1998).
5. Gnoffo, P. A., Planetary entry gas dynamics. *Annu. Rev. Fluid Mech.* 1999, **31**, 459–494.
6. Monteverde, F. and Bellosi, A., Advances in microstructure and mechanical properties of zirconium diboride-based ceramics. *Mater. Sci. Eng.* 2003, **A346**, 310–319.
7. Metcalfe, A. G., Elsner, D. T., Allen, D. T., Wuchina, E., Opeka, M. and Opila E., Oxidation of hafnium diboride. In *High Temperature Corrosion and Materials Chemistry: Per Kofstad Memorial Symposium, Electrochemical Society Proceedings, Vol 99-38*. pp. 489–501.
8. Monteverde, F. and Bellosi, A., Oxidation of ZrB_2 based ceramics in dry air. *J. Electrochem. Soc.* 2003, **150**(11), B552–B559.
9. Bellosi, A. and Monteverde, F., Fabrication and properties of zirconium diboride based ceramics for UHT applications. In *Proceedings of the 4th European Workshop 'Hot Structures and TPS for Space Vehicles'*. ESA-SP521, 2003. pp. 65–71.
10. Monteverde, F. and Bellosi, A., Microstructure and properties of an HfB_2–SiC composite for ultra high temperature applications. *Adv. Eng. Mater.* 2004, **6**(5), 331–336.
11. Nickel, K. G., Multiple law modelling for the oxidation of advanced ceramics and a model-independent figure of merit. In *Corrosion of Advanced Ceramics/Measurements and Modelling*, ed. K. G. Nickel. Kluwer Academic Publishers, Dordrecht, The Netherlands, 1994, pp. 59–71.
12. Hilfer, G., The impact of environmental conditions during re-entry of the re-usability of a Si-based ceramic TPS. In *Proceedings of the 4th European Workshop 'Hot Structures and TPS for Space Vehicles'*. ESA-SP521, 2003, pp. 363–368.
13. Hinze, J. W., Tripp, W. C. and Graham, H. C., The high temperature oxidation behaviour of a HfB_2 + 20 v/o SiC composite. *J. Electrochem. Soc.* 1975, **122**(9), 1249–1254.
14. Tripp, W. C., Davis, H. H. and Graham, H. C., Effect of an SiC addition on the oxidation of ZrB_2. *Am. Ceram. Soc. Bull.* 1973, **52**(8), 612–616.
15. Levine, S. R., Opila, E. J., Halbig, M. C., Kiser, J. D., Singh, M. and Salem, J. A., Evaluation of ultra high temperature ceramics for aeropropulsion use. *J. Eur. Ceram Soc.* 2002, **22**, 2757–2767.